American Mineralogist, Volume 100, pages 1040–1046, 2015

SPECIAL COLLECTION: APATITE: A COMMON MINERAL, UNCOMMONLY VERSATILE

Thermal expansion of F-Cl apatite crystalline solutions† 🔓

GUY HOVIS[1,*], TONY ABRAHAM[2], WILLIAM HUDACEK[3], SARAH WILDERMUTH[4], BRIAN SCOTT[1], CAITLIN ALTOMARE[5], AARON MEDFORD[6], MARICATE CONLON[7], MATTHEW MORRIS[1], AMANDA LEAMAN[1], CHRISTINE ALMER[1], GARY TOMAINO[8] AND DANIEL HARLOV[9]

[1]Department of Geology and Environmental Geosciences, Lafayette College, Easton, Pennsylvania 18042, U.S.A.
[2]Department of Earth Sciences, University of Cambridge, 10 Downing Street, Cambridge CB2 3EQ, U.K.
[3]MAT Program, American Museum of Natural History, Central Park West at 79th Street, New York, New York 10024, U.S.A.
[4]Department of Geology, University of Kansas, Lawrence, Kansas 66045, U.S.A.
[5]Weiss School of Natural Sciences, Rice University, Houston 77251, Texas, U.S.A.
[6]School of Earth and Climate Sciences and Climate Change Institute, University of Maine, Orono, Maine 04469, U.S.A.
[7]ENVIRON, 214 Carnegie Center, Princeton, New Jersey 08540, U.S.A.
[8]Specialty Minerals Inc., 640 North Thirteenth Street, Easton, Pennsylvania 18042, U.S.A.
[9]Deutsches GeoForschungsZentrum Potsdam, Telegrafenberg, D-14473 Potsdam, Germany

ABSTRACT

We have studied the thermal expansion of 15 synthetic and two natural F-Cl apatite solid solutions through the calculation of unit-cell dimensions at elevated temperatures based on X-ray powder diffraction data collected from room temperature to ~900 °C at 50 to 100 °C intervals. Coefficients of thermal expansion for the *a* and *c* unit-cell axes show sensitivity to composition, with α_a increasing by about 50% and α_c decreasing by a third from chlorapatite to fluorapatite. Despite the relationships observed for *a* and *c*, the thermal expansion coefficient for unit-cell volume shows little sensitivity to composition, which can be explained only by a mutually compensating structural adjustment along the latter axes as temperature rises. Results of this study also imply that the thermodynamically ideal volumes of mixing for F-Cl apatite solid solutions observed at ambient conditions continue to at least 900 °C.

Keywords: Fluorapatite, chlorapatite, thermal expansion, thermodynamic properties

INTRODUCTION

Apatite, $A_5(XO_4)_3Z$, is a common mineral that occurs in igneous, metamorphic, and sedimentary rocks. Additionally, it is an important component of planetary materials (Piccoli and Candela 2002; Spear and Pyle 2002; Knudsen and Gunter 2002; Patiño Douce and Roden 2006; Jones et al. 2014), having been used to estimate H_2O abundances in the interiors of the Moon and Mars (McCubbin et al. 2010a, 2010b, 2011, 2012; Gross et al. 2013). Apatite is the main hard part of the human anatomy, the source of phosphorous in fertilizer, and an important potential material for the storage of nuclear waste (Ewing and Wang 2002). Understanding fundamental properties of the apatite mineral group is of significant interest, therefore, to the fields of geology, biology, medicine, planetary science, and materials science.

Numerous chemical substitutions occur in this complex mineral system. Although the primary occupants of the A and X sites are Ca^{2+} and P^{5+}, respectively, natural specimens can display substitutions of REE^{3+}, Sr^{2+}, and Na^{+} in A; S^{6+}, Si^{4+}, and C^{4+} in X; and F^{-}, Cl^{-}, $(OH)^{-}$, O^{2-}, $(CO_3)^{2-}$, and S^{2-} in Z (Pan and Fleet 2002; Hovis and Harlov 2010; Boyce et al. 2010; Gross and Berndt 2002).

Despite the importance of apatite as an Earth material, basic thermodynamic data are nonexistent for much of the system, especially for compositions between end-members. In our initial studies of apatite thermodynamics, the goal has been to investigate behavior of the main anion substitutions in $Ca(PO_4)_3Z$ apatite, namely F, Cl, and OH, noting that fluorapatite is the most commonly occurring member of this mineral group in rocks. In this regard, Hovis and Harlov (2010) reported on the enthalpy-of-mixing behavior for F-Cl binary apatites. This was followed by investigation of F-OH apatite enthalpies and volumes of mixing (Hovis et al. 2014a). The third contribution to this work concerned thermal expansion data for the F-OH apatite system (Hovis et al. 2014b). In the current paper, we report on thermal expansion properties of the synthetic F-Cl apatite specimens studied by Hovis and Harlov (2010), as well as natural samples of the F, Cl, and OH end-members.

METHODOLOGY

Sample synthesis

Synthesis of F-Cl apatite crystalline solutions took place at the GeoForschungs-Zentrum-Potsdam (GFZ) using the slow-cooled, molten flux method described by Cherniak (2000) and Prener (1967). As described by Hovis and Harlov (2010) and Schettler et al. (2011), the flux consisted of molar amounts of thoroughly mixed, fine powders of CaF_2 and $CaCl_2$ in variable proportions such

* E-mail: hovisguy@lafayette.edu

† 🔓 Open access: Article available to all readers online. Special collection papers can be found on GSW at http://ammin.geoscienceworld.org/site/misc/specialissuelist.xhtml.

0003-004X/15/0506–1040$05.00/DOI: http://dx.doi.org/10.2138/am-2015-5176

that they summed to 0.1 mol × CaF_2 + (1 – x)$CaCl_2$ or about 10 to 11 g total. A fine $Ca_3(PO_4)_2$ powder (0.03 mol or 9.305 g) was then mechanically dry mixed into the flux. Because F strongly partitions into apatite, for all intermediate compositions the flux consisted principally of $CaCl_2$ with minor amounts of CaF_2. Either pure $CaCl_2$ or CaF_2 was utilized as a flux for end-member chlorapatite or fluorapatite, respectively. The dry mix was packed into a 30 mL volume Pt crucible and pressed down using the pestle. The Pt crucible, with a loose fitting Pt cover, was then placed in a programmable high-temperature oven and the temperature ramped to 1375 °C over a period of 4 h. The melt was allowed to equilibrate or "soak" at 1375 °C for 15 h, then slowly cooled to 1220 °C at a rate of 3 °C/h during which fluor-chlorapatite crystals nucleated and grew in the melt. After 1 to 20 h at 1220 °C, the crucible was removed from the oven and quenched in air for about 30 min until it was cool enough to extract the flux-crystal mass as a solid lump. The fluor-chlorapatite crystals were separated from the flux by boiling the quenched product in distilled water in a 2 L beaker. If the flux contained more than a few percent by weight CaF_2, the flux + crystals were boiled in an aqueous 20% solution of $Al(NO_3)_3 \cdot 9H_2O$ to dissolve the residual CaF_2. The resulting transparent, inclusion-free, light blue-green, euhedral–semi-euhedral fluor-chlorapatite crystals ranged in length from 100 μm up to 6–7 mm in length and from 20 μm to 3–4 mm in diameter.

The compositions of each of the fluor-chlorapatite samples synthesized for the original study were carefully determined by wet chemical means as discussed in detail by Schettler et al. (2011). In general, the principal differences in composition among the various apatite samples are their F:Cl ratios. However, compositions for the Cl-rich third of the compositional range contain nontrivial amounts of oxyapatite [$Ca_5(PO_4)_3O_{0.5}$] (ibid). Indeed, natural F-Cl apatites containing an oxyapatite component have been described by Young and Munson (1966).

In addition to the samples synthesized at GFZ-Potsdam, thermal expansion measurements have been made on three natural apatite samples: chlorapatite, American Museum of Natural History specimen AMNH 23101 from Kragerø, Norway; fluorapatite, National Museum of Natural History specimen NMNH 144954-3, from Durango, Mexico; and hydroxylapatite, National Museum of Natural History specimen NMNH R9498, from Holly Springs, Georgia, U.S.A. The chlorapatite composition, $(Ca_{4.88}Fe_{0.01}Na_{0.08}Ce_{0.01})(P_{3.01}O_{12})(F_{0.09}Cl_{0.91})$, given by Hughes et al. (1989) is based on electron microprobe and INAA analyses. The fluorapatite analysis, $(Ca_{4.97}Na_{0.04}Ce_{0.02})(P_{2.98}Si_{0.01}S_{0.02}O_{12})(F_{0.92}Cl_{0.06}OH_{0.03})$, was performed by Francis McCubbin at the University of New Mexico using continuous flow mass spectrometry for H_2O determination and specialized electron-probe microanalysis for fluorine, as described in Hovis et al. (2014a). [Also see the composition of Young et al. (1969) on a different (but related) sample of Durango fluorapatite.] That for NMNH R9498, $[Ca_{5.00}(P_{3.00}O_{12.00})(F_{0.09}Cl_{0.04}(OH)_{0.89})]$, also analyzed by McCubbin, is given in Table 1 of Hovis et al. (2014b).

Thermal expansion data for the natural fluorapatite and hydroxylapatite samples were given previously in Hovis et al. (2014b), but those for chlorapatite AMNH 23101 are given here for the first time.

High-temperature X-ray powder diffraction measurements

The thermal expansion research involved subjecting powdered apatite samples to Cu*K*α X-radiation at a series of temperatures, then using the diffraction data to calculate unit-cell dimensions of the samples at each temperature. The research extended over a several-year period. Initial measurements were made during several short-term visits to the University of Cambridge, U.K., on a Bruker D8 θ-θ system having high-temperature capability; digital data were brought back to Lafayette College for analysis using IGOR spectral-analysis software. More recent work on natural chlorapatite, fluorapatite, and hydroxylapatite specimens were made at Lafayette College on a newly-acquired PANalytical Empyrean θ-θ X-ray diffractometer equipped with a PIXEL 3D detector and an Anton Parr HTK 1200N furnace. In the transitional year between the Cambridge- and Lafayette-based work, high-temperature measurements were made at Specialty Minerals Inc. (Easton, Pennsylvania) on a Rigaku Ultima θ-θ system. X-ray data from both the Rigaku and PANalytical systems consisted of direct output produced by system software and did not require IGOR analysis. Note that the measurement site and XRD unit utilized for each sample are included in Tables 1[1] and 2.

For measurements made in Cambridge, temperature calibration of the Bruker system was limited by the short-term nature of our visits. Temperatures were checked via the high/low quartz transition and generally found to be within ~20–30 °C of the set temperature. However, having no basis for temperature corrections at additional temperatures, no temperature corrections have been made to the Cambridge data. As documented below, duplicate experiments made on systems that were better-calibrated for temperature have allowed us to confirm the temperature integrity of the earlier data.

For the Rigaku-based measurements made at Specialty Minerals Inc., sample temperatures were checked through a set of experiments that utilized reversible phase transformations for KNO_3, $KClO_4$, K_2SO_4, K_2CrO_4, $BaCO_3$, and $SrCO_3$, collectively resulting in temperature calibration from ~115 to 930 °C. Based on the latter, it is estimated that the set-point temperatures for the Rigaku-based XRD measurements are correct to ±15 °C.

X-ray measurements made at Lafayette College with the PANalytical system were calibrated for temperature utilizing the same methodology as for the Rigaku system using KNO_3, $KClO_4$, K_2SO_4, and $BaCO_3$, resulting in calibration measurements taken between ~115 and 800 °C. Based on the latter, it was determined that actual temperatures were approximately 25 to 30 °C higher than the set-point values; results in the data tables and figures of this paper reflect the corrected temperatures.

Apatite peak positions were corrected through use of National Institute of Standards and Technology (NIST) sample SRM 640a silicon (with a stated unit-cell dimension of 5.430825 Å), which was mixed with each sample. High-temperature Si peak positions were based on the Si thermal expansion data of Parrish (1953). Unit-cell dimension calculations for all data utilized the software of Holland and Redfern (1997). The indexing of apatite peaks at elevated temperatures simply involved tracking known peaks at room temperature to higher temperatures utilizing data for both F and Cl apatite end-members.

Results

Unit-cell results for all samples are reported in Table 1[1]. This table also records the X-ray unit on which each data set was collected (Cambridge University/Bruker D8, Specialty Minerals/Rigaku Ultima, Lafayette College/PANalytical Empyrean). Note that duplicate experiments were conducted on samples APS21, APS25, APS26, APS27, and APS36 to check early Cambridge-based unit-cell parameters against later results based on temperature calibrations that were more thorough. Figure 1 demonstrates good internal consistency among the data.

For the most part, apatite-group minerals display hexagonal symmetry. However, the powder diffraction methods used here did not allow distinction between hexagonal and monoclinic symmetry for Cl-rich samples (e.g., Mackie et al. 1972). Even when present, monoclinic symmetry for the latter is reflected by only a minute departure (≤0.06°) from a γ interaxial angle of 120° (e.g., note the data of Hounslow and Chao 1970).

Figures 2 to 4 show plots of unit-cell volume (*V*), *a*, and *c*, respectively, against temperature. For the sake of clarity, we have chosen not to plot all data that were collected, but rather representative data for 10 (of the 15 different) series at more-or-less regular compositional intervals. The parameters for both linear and quadratic fits to *V*, *a*, and *c* as a function of temperature, along with R^2 for each, are given for all series in Table 2. It is evident that quadratic fits to *V*, *a*, and *c* as a function of temperature are statistically justified in many cases. Nevertheless, the linear fits for *V* and *a* shown in Figures 2 and 3 do well in fitting the data. Relationships for the *c* dimension (Fig. 4), on the other hand, are generally more curved and better fit by quadratic relationships.

For a general comparison of samples in terms of the degree to which they expand, it is useful to compare either the slopes of linear least-squares fits to the data on the various graphs or the coefficients of thermal expansion, which are calculated for volume as

[1] Deposit item AM-15-55176, Table 1. Deposit items are stored on the MSA web site and available via the American Mineralogist Table of Contents. Find the article in the table of contents at GSW (ammin.geoscienceworld.org) or MSA (www.minsocam.org), and then click on the deposit link.

TABLE 2. Thermal expansion equations for apatite solid solutions

Sample no., XRD unit[a]	Mole fraction F and F+OH[b]	Order of least-squares fit	Unit-cell volume (Å³) equation coefficients					Unit-cell dimension *a* (Å) equation coefficients				
			a_0	a_1	a_2	α_V x 10^6 (deg^{-1})	R^2	a_0	a_1	a_2	α_a x 10^6 (deg^{-1})	R^2
APS25, CB	1.017[c]	linear	522.13	2.1668E-02		41.5	0.9916	9.3620	1.2958E-04		13.8	0.9919
APS25, CB	1.017[c]	quadratic	523.19	1.4876E-02	6.7096E-06		0.9986	9.3677	9.3080E-05	3.6053E-08		0.9976
APS25, SR	1.017[c]	linear	522.82	2.1105E-02		40.4	0.9986	9.3665	1.2573E-04		13.4	0.9978
APS25, SR	1.017[c]	quadratic	522.97	2.0112E-02	1.0465E-06		0.9988	9.3675	1.1957E-04	6.4970E-09		0.9980
NMNH 144954-3, LP	0.92/0.95[b]	linear	524.81	2.2198E-02		42.3	0.9972	9.3873	1.3134E-04		14.0	0.9984
NMNH 144954-3, LP	0.92/0.95[b]	quadratic	525.51	1.7692E-02	4.7625E-06		0.99996	9.3904	1.1148E-04	2.0985E-08		0.9999
APS21, CB	0.890	linear	525.86	2.1871E-02		41.6	0.9975	9.3983	1.2766E-04		13.6	0.9973
APS21, CB	0.890	quadratic	525.94	2.1372E-02	5.2578E-07		0.9976	9.3971	1.3580E-04	–8.5881E-09		0.9975
APS21, SR	0.890	linear	525.63	2.1542E-02		41.0	0.9978	9.3973	1.2471E-04		13.3	0.9935
APS21, SR	0.890	quadratic	525.26	2.3909E-02	–2.4961E-06		0.9986	9.3933	1.5085E-04	–2.7554E-08		0.9965
APS20, CB	0.849	linear	526.54	2.1472E-02		40.8	0.9949	9.4111	1.2500E-04		13.3	0.9962
APS20, CB	0.849	quadratic	527.32	1.6281E-02	5.4390E-06		0.9985	9.4141	1.0491E-04	2.1055E-08		0.9978
APS18, CB	0.741	linear	528.93	2.2547E-02		42.6	0.9973	9.4367	1.2996E-04		13.8	0.9967
APS18, CB	0.741	quadratic	529.13	2.0940E-02	1.9724E-06		0.9977	9.4365	1.3166E-04	–2.0911E-09		0.9967
APS27, CB	0.665	linear	530.14	2.2521E-02		42.5	0.9939	9.4525	1.2914E-04		13.7	0.9951
APS27, CB	0.665	quadratic	530.86	1.7442E-02	5.8049E-06		0.9973	9.4554	1.0912E-04	2.2875E-08		0.9968
APS27, SR	0.665	linear	530.87	2.1695E-02		40.9	0.9985	9.4581	1.2167E-04		12.9	0.9967
APS27, SR	0.665	quadratic	530.85	2.1796E-02	–1.0582E-07		0.9985	9.4556	1.3791E-04	–1.7128E-08		0.9979
APS34, CB	0.565	linear	532.51	2.3475E-02		44.1	0.9973	9.4792	1.3394E-04		14.1	0.9979
APS34, CB	0.565	quadratic	532.91	2.0260E-02	3.9456E-06		0.9987	9.4798	1.2917E-04	5.8615E-09		0.9980
APS35, CB	0.434	linear	535.15	2.3559E-02		44.0	0.9986	9.5108	1.3105E-04		13.8	0.9984
APS35, CB	0.434	quadratic	535.36	2.1876E-02	2.0653E-06		0.9990	9.5105	1.3363E-04	–3.1715E-09		0.9985
APS23, CB	0.40	linear	534.28	2.2446E-02		42.0	0.9967	9.5103	1.2232E-04		12.9	0.9965
APS23, CB	0.40	quadratic	534.79	2.0162E-02	2.0761E-06		0.9970	9.5101	1.2320E-04	–8.0808E-10		0.9965
APS36, CB	0.372	linear	536.79	2.3523E-02		43.8	0.9972	9.5346	1.2575E-04		13.2	0.9981
APS36, CB	0.372	quadratic	537.29	1.9942E-02	3.9201E-06		0.9988	9.5351	1.2180E-04	4.3223E-09		0.9981
APS36, SR	0.372	linear	536.94	2.2291E-02		41.5	0.9996	9.5354	1.1507E-04		12.1	0.9961
APS36, SR	0.372	quadratic	537.02	2.1770E-02	5.4916E-07		0.9997	9.5320	1.3681E-04	–2.2915E-08		0.9986
APS16, CB	0.244[d]	linear	537.82	2.3105E-02		43.0	0.9960	9.5470	1.2247E-04		12.8	0.9960
APS16, CB	0.244[d]	quadratic	538.31	1.9635E-02	3.7987E-06		0.9976	9.5489	1.0914E-04	1.4593E-08		0.9969
APS29, CB	0.16[d]	linear	539.28	2.2824E-02		42.3	0.9977	9.5718	1.1518E-04		12.0	0.9981
APS29, CB	0.16[d]	quadratic	539.72	1.9642E-02	3.4830E-06		0.9991	9.5731	1.0632E-04	9.6972E-09		0.9986
AMNH 23101, LP	0.09/0.09[b]	linear	541.69	2.2833E-02		42.2	0.9981	9.6061	1.0682E-04		11.1	0.9988
AMNH 23101, LP	0.09/0.09[b]	quadratic	542.19	1.9641E-02	3.3731E-06		0.9995	9.6055	1.1099E-04	–4.4043E-09		0.9989
NMNH R9498, LP	0.09/0.97[b]	linear	528.15	2.2891E-02		43.3	0.9978	9.4221	1.3472E-04		14.3	0.9992
NMNH R9498, LP	0.09/0.97[b]	quadratic	528.77	1.8891E-02	4.2266E-06		0.9998	9.4237	1.2457E-04	1.0727E-08		0.9996
APS15, CB	0.083[d]	linear	541.07	2.1732E-02		40.2	0.9974	9.5980	1.0820E-04		11.3	0.9950
APS15, CB	0.083[d]	quadratic	541.45	1.8800E-02	3.6732E-06		0.9986	9.6005	8.8944E-05	2.4124E-08		0.9972
APS30, CB	0.059[d]	linear	541.42	2.2069E-02		40.8	0.9928	9.6054	9.8565E-05		10.3	0.9936
APS30, CB	0.059[d]	quadratic	542.31	1.6331E-02	5.6655E-06		0.9976	9.6074	8.6116E-05	1.2293E-08		0.9947
APS24, CB	0.037[d]	linear	542.20	2.1759E-02		40.1	0.9920	9.6196	9.7711E-05		10.2	0.9881
APS24, CB	0.037[d]	quadratic	543.07	1.6118E-02	5.9482E-06		0.9966	9.6233	7.3800E-05	2.5211E-08		0.9922
APS26, CB	0.002[d]	linear	542.96	2.2752E-02		41.9	0.9972	9.6296	9.2418E-05		9.6	0.9970
APS26, CB	0.002[d]	quadratic	543.52	1.8801E-02	4.3252E-06		0.9994	9.6296	9.2814E-05	–4.3306E-10		0.9970
APS26, SR	0.002[d]	linear	543.91	2.0746E-02		38.1	0.9986	9.6630	8.7264E-05		9.0	0.9978
APS26, SR	0.002[d]	quadratic	544.05	1.9798E-02	9.9955E-07		0.9988	9.6632	8.6496E-05	8.1012E-10		0.9978

Notes: Equations have the form V or a or $c = a_0 + a_1 T + a_2 T^2$, where T is temperature (°C); values of thermal expansion coefficients, α, are based on linear fits to the data and calculated as in Equation 1. Equations for unit-cell volume for natural fluorapatite NMNH 144954-3 and hydroxylapatite NMNH R9498 have been given previously in Hovis et al. (2014b), but equations for a and c are presented here for the first time.

[a] Institutions and X-ray units utilized: CB = University of Cambridge, Bruker D8; SR = Specialty Minerals Inc., Rigaku Ultima; LP = Lafayette College, PANalytical Empyrean

[b] Natural samples contain F, OH, and Cl, whereas the IR spectra of Schettler et al. (2011) indicate no discernable OH in F-Cl synthetic (APS) apatite samples.

[c] F > 1.0 determined by Schettler et al. (2011).

[d] The sample appears to contain an oxyapatite component (Table 4 of Schettler et al. 2011).

Table extends to next page

$$\alpha_V = (\Delta V/\Delta T)/V_{0°C} \quad (1)$$

where $\Delta V/\Delta T$ is the slope of the fit and $V_{0°C}$ is the intercept of the same fit at 0 °C. The latter are included in Table 2.

It is instructive to plot the thermal expansion coefficients for V, a, and c (the latter two calculated in a manner comparable to that for V) against composition (Figs. 5 through 7). Figure 5 demonstrates that the thermal expansion coefficient for volume is affected little, if at all, by F:Cl ratio; this is reflected as well by the parallelism of V-T data for the various samples on Figure 2. Figures 6 and 7, on the other hand, show clearly that thermal expansion coefficients for the individual unit-cell axes a and c are a function of composition, α_a increasing and α_c decreasing as fluorine content rises. The systematic behavior of $\Delta c/\Delta T$ relations with composition also is readily evident from relationships in Figure 4, where values of c among all series display greater convergence at high than at low temperature. Thus, volume, which is itself a function of the a and c unit-cell lengths, behaves differently than the axes themselves.

In Figures 5 to 7, we have included data for the thermal expansion coefficients of F-OH apatite solid solutions based on the recent results of Hovis et al. (2014b). Note that although values of α_V for F-OH apatites may generally fall slightly below those of F-Cl solutions (Fig. 5), there is general overlap and a

TABLE 2.—*EXTENDED*

Unit-cell dimension *c* (Å) equation coefficients				
a_0	a_1	a_2	$\alpha_c \times 10^6$ (deg^{-1})	R^2
6.8793	9.1079E-05		13.2	0.9914
6.8841	6.0736E-05	2.9975E-08		0.9994
6.8817	8.9544E-05		13.0	0.9988
6.8818	8.9059E-05	5.1191E-10		0.9988
6.8775	9.4541E-05		13.7	0.9950
6.8814	6.9104E-05	2.6879E-08		0.9999
6.8751	9.5420E-05		13.9	0.9950
6.8773	8.0848E-05	1.5364E-08		0.9966
6.8734	9.5722E-05		13.9	0.9968
6.8740	9.1478E-05	4.4746E-09		0.9969
6.8653	9.3905E-05		13.7	0.9903
6.8704	6.0178E-05	3.5343E-08		0.9983
6.8589	1.0004E-04		14.6	0.9952
6.8613	8.0665E-05	2.3780E-08		0.9978
6.8517	1.0017E-04		14.6	0.9880
6.8563	6.8085E-05	3.6666E-08		0.9950
6.8530	1.0021E-04		14.6	0.9957
6.8559	8.1371E-05	1.9862E-08		0.9981
6.8438	1.0448E-04		15.3	0.9931
6.8476	7.3973E-05	3.7451E-08		0.9991
6.8319	1.0892E-04		15.9	0.9941
6.8345	8.7940E-05	2.5756E-08		0.9968
6.8220	1.0672E-04		15.6	0.9948
6.8279	8.0231E-05	2.4077E-08		0.9970
6.8188	1.1499E-04		16.9	0.9914
6.8238	7.9512E-05	3.8830E-08		0.9982
6.8196	1.1491E-04		16.8	0.9934
6.8248	8.0751E-05	3.6108E-08		0.9995
6.8141	1.1414E-04		16.8	0.9958
6.8169	9.3636E-05	2.2446E-08		0.9981
6.7971	1.2047E-04		17.7	0.9960
6.8004	9.6918E-05	2.5780E-08		0.9987
6.7789	1.3133E-04		19.4	0.9928
6.7855	8.9381E-05	4.4330E-08		0.9997
6.8702	9.7215E-05		14.2	0.9923
6.8753	6.4550E-05	3.4517E-08		0.9999
6.7824	1.1681E-04		17.2	0.9981
6.7832	1.1012E-04	8.3820E-09		0.9983
6.7765	1.3348E-04		19.7	0.9983
6.7844	8.3196E-05	4.9651E-08		0.9984
6.7662	1.3074E-04		19.3	0.9940
6.7713	9.8035E-05	3.4484E-08		0.9984
6.7617	1.5023E-04		22.2	0.9921
6.7682	1.0388E-04	5.0734E-08		0.9989
6.7685	1.3269E-04		19.6	0.9972
6.7697	1.2484E-04	8.2812E-09		0.9974

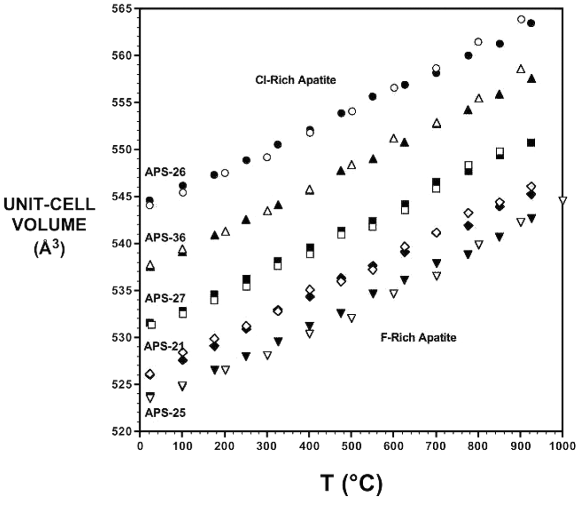

FIGURE 1. Unit-cell volume vs. temperature (°C) for five synthetic F-Cl apatite specimens studied at the University of Cambridge (open symbols) and also at Specialty Minerals Inc. (solid symbols) to check data consistency between XRD systems. Plotted temperatures reflect temperature calibrations discussed in the text. Widths of the symbols equate to about 0.8 Å^3, several times larger than standard errors given in Table 1[1].

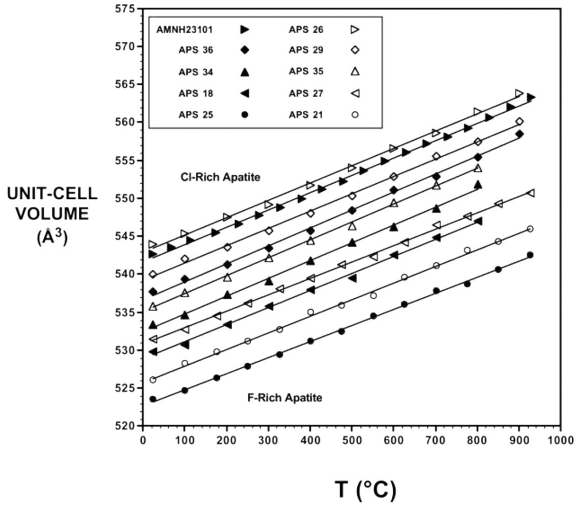

FIGURE 2. Unit-cell volume (Å^3) vs. temperature (°C) for 10 of the chlor-fluorapatite specimens studied during this investigation, seven measured in Cambridge, two (APS-27 and APS-25) at Specialty Minerals Inc., and one (AMNH-23101) at Lafayette College. Data for these and other specimens are given in Table 1[1]. Plotted temperatures reflect temperature calibrations discussed in the text. Widths of the symbols equate to about 0.8 Å^3, several times larger than standard errors given in Table 1[1]. Equations for the fitted lines are given in Table 2.

lack of compositional variability among data for both the F-Cl and F-OH series. The same is not true, however, for the thermal expansion coefficients related to *a* and *c* (Figs. 6 and 7), at least for F-Cl apatite solutions.

DISCUSSION

Generally, Figure 5 demonstrates that there is little sensitivity of volume expansion to composition shown by F, Cl, and OH apatite end-members, nor by intermediate members of the F-Cl and F-OH apatite series. This means that the ideal thermodynamic mixing behavior related to volume for F-Cl (Fig. 8) and F-OH (Hovis et al. 2014b, their Fig. 3) apatite series extends from room temperature to at least 900 °C, although admittedly there is some uncertainty in interpretation of F-Cl apatite volumes due to the presence of an oxyapatite component in Cl-rich samples.

One can surmise that the insensitivity of volume expansion to F:Cl:OH ratio is related to the seemingly insignificant role of the anion in the apatite structure, as the latter constitutes just one of six ions that coordinate the so-designated Ca(2) position in the structure (Hughes et al. 1989; also see Hughes and Rakovan 2002, for multiple additional references), the remaining five being O^{2-}. From Figures 6 and 7, however, it is clear that the anion does indeed make a difference to expansion along the individual unit-cell axes, where α_a increases by about 50% from the Cl- to

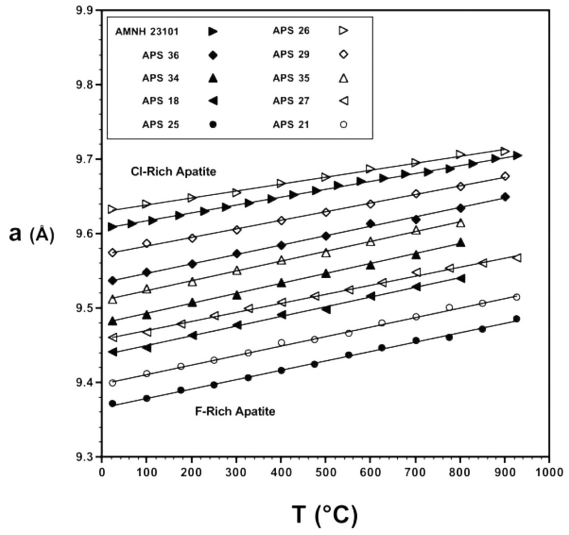

Figure 3. Unit-cell dimension *a* (Å) vs. temperature (°C) for the same 10 chlor-fluorapatite specimens shown in Figure 2. Data for these and other specimens are given in Table 1[1]. Plotted temperatures reflect temperature calibrations discussed in the text. Widths of the symbols equate to about 0.004 Å, several times larger than the standard errors given in Table 1[1]. Equations for the fitted lines are given in Table 2.

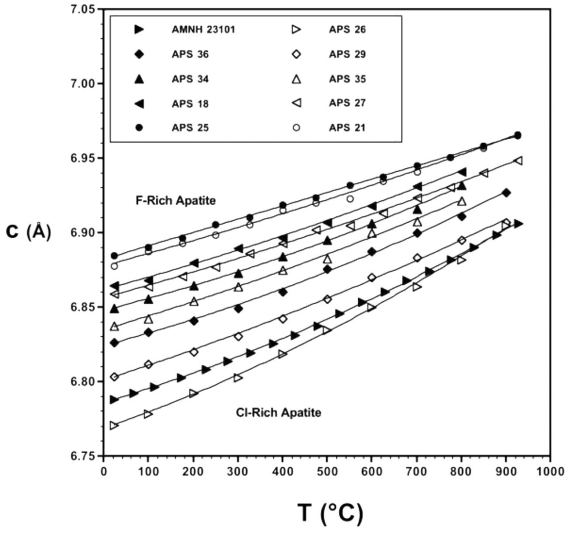

Figure 4. Unit-cell dimension *c* (Å) vs. temperature (°C) for the same 10 chlor-fluorapatite specimens shown in Figure 2. Data for these and other specimens are given in Table 1[1]. Plotted temperatures reflect temperature calibrations discussed in the text. Sizes of the symbols equate to about 0.003 Å, several times larger than the standard errors given in Table 1[1]. Equations for the fitted curves are given in Table 2.

the F-end of the apatite series as α_c decreases by about a third over the same range.

One is tempted to ascribe the observed sensitivity of α_a, seen mainly in the Cl-rich third of the compositional range (Fig. 6), to the oxyapatite substitution described by Schettler et al. (2011) for Cl-rich samples. We reject such interpretation, however, for

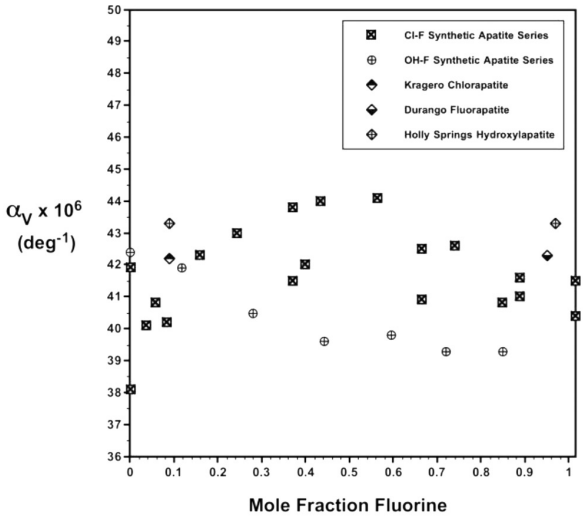

Figure 5. Thermal expansion coefficients for unit-cell volume (Table 2) plotted against mole fraction fluorine for all synthetic F-Cl apatite specimens (Hovis and Harlov 2010) and natural chlorapatite AMNH-23101 studied during the present investigation. Compositions for the synthetic apatites are from Schettler et al. (2011). For comparison, data also are shown for synthetic F-OH specimens, as well as natural fluorapatite (NMNH 144954-3) and hydroxylapatite (NMNH R9498) as given in Hovis et al. (2014b). For natural fluorapatite (which contains little OH) composition is plotted as X_{F+OH}, but for natural hydroxylapatite composition is plotted twice, both as X_F and X_{F+OH}.

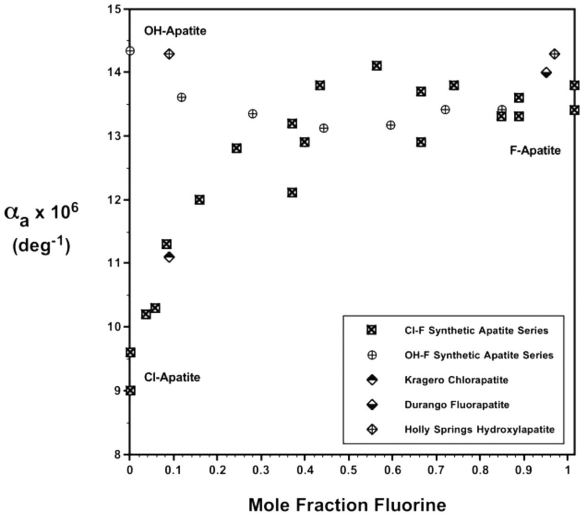

Figure 6. Thermal expansion coefficients for the *a* unit-cell dimension (Table 2) plotted against mole fraction fluorine for all synthetic F-Cl apatite specimens (Hovis and Harlov 2010) and natural chlorapatite AMNH-23101 studied during the present investigation. Compositions for the synthetic apatites are from Schettler et al. (2011). For comparison, data also are shown for synthetic F-OH specimens, as well as natural fluorapatite (NMNH 144954-3) and hydroxylapatite (NMNH R9498) as given in Hovis et al. (2014b). For natural fluorapatite (which contains little OH) composition is plotted as X_{F+OH}, but for natural hydroxylapatite composition is plotted twice, both as X_F and X_{F+OH}.

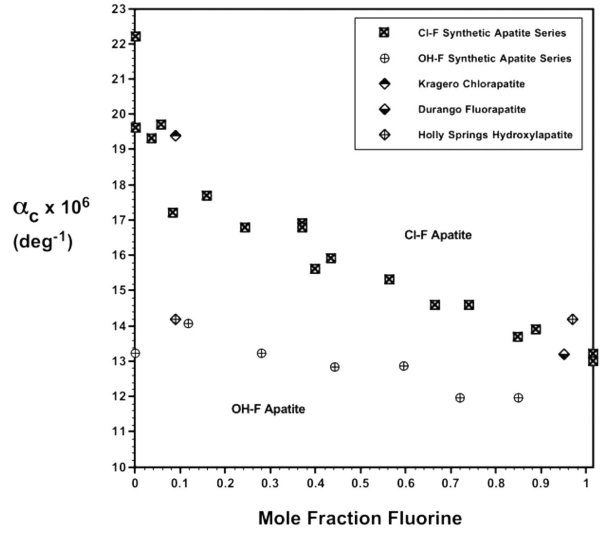

FIGURE 7. Thermal expansion coefficients for the *c* unit-cell dimension (Table 2) plotted against mole fraction fluorine for all synthetic F-Cl apatite specimens (Hovis and Harlov 2010) and chlorapatite AMNH-23101 studied during the present investigation. Compositions for the synthetic apatites are from Schettler et al. (2011). For comparison, data also are shown for synthetic F-OH specimens, as well as natural fluorapatite (NMNH 144954-3) and hydroxylapatite (NMNH R9498) as given in Hovis et al. (2014b). For natural fluorapatite (which contains little OH) composition is plotted as X_{F+OH}, but for natural hydroxylapatite composition is plotted twice, both as X_F and X_{F+OH}.

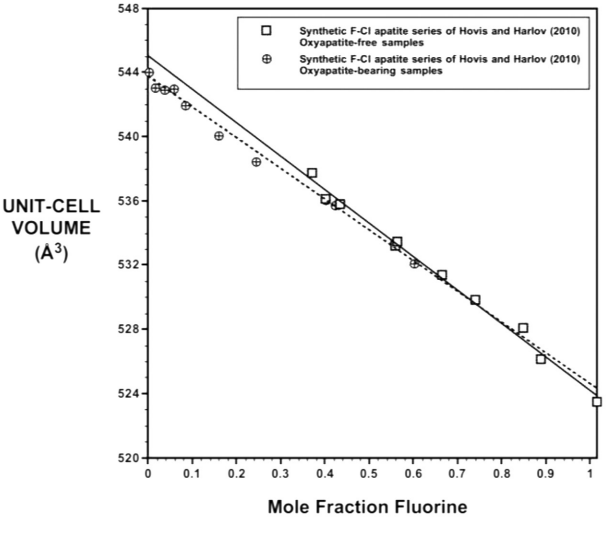

FIGURE 8. Room-temperature unit-cell volumes for the synthetic Cl-F apatite specimens of Hovis and Harlov (2010), as measured at Lafayette College, plotted against mole fraction fluorine for the same specimens from Schettler et al. (2011). The solid line, V (Å^3) = 545.06–20.867 X_F (R^2 = 0.9922), is based only on data for oxyapatite-free samples, whereas the dashed line, V (Å^3) = 543.78–19.169 X_F (R^2 = 0.9934), is based on data for all specimens; as given, either relationship reflects ideal thermodynamic Cl-F mixing. If the presence of an oxyapatite component has no effect on volume, then nonideal volumes of mixing for the series would be implied, but there is no information upon which to base such a judgment.

several reasons. One is that the amount of oxyapatite substitution varies considerably among Cl-rich samples (ibid), whereas related variability in α_a data is not evident. Another is that data for natural chlorapatite AMNH 23101 and hydroxylapatite NMNH R9498 fit well with those of synthetic Cl-rich and OH-rich samples, respectively. And, finally, compositional variability for α_c is seen over the entire compositional range (Fig. 7), not just for Cl-rich samples. It seems clear, then, that thermal expansion along *a* and *c* must involve a cooperative and inverse structural relationship that depends mainly upon F:Cl ratio.

Hughes et al. (2014) recently have discussed in detail the anion arrangements of F^- and Cl^- in fluor-chlorapatite solid solutions. Based on structure, it seems that there are at least two possible explanations for the cooperative relationship between *a* and *c* during thermal expansion. One is that thermal ellipsoids of the anions, and perhaps other ions as well, change with heating. A second possibility is that the positioning (and/or arrangement) of anions in the apatite anion column changes with temperature. Unfortunately, however, we know of no single-crystal work on apatite-group minerals at elevated temperatures that might help clarify the observed relationships.

Finally, one can ask why the F:Cl-dependent relationship between α_a and α_c for the fluor-chlorapatite system is not observed as much, or at all, in F-OH apatite solid solutions. It seems likely that this is related to anion size differences, where OH^- and F^- are approximately the same size, but Cl^- is considerably larger than either of the latter. On the other hand, size arguments relative to anions in the apatite structure can be misleading, as Cl-bearing chlorapatite displays a smaller *c* dimension than F-bearing fluorapatite (Fig. 4), despite parallelism of the anion column to the *c* axis.

IMPLICATIONS

It is our hope that full thermodynamic characterization of apatite-group minerals will lead to the successful use of these minerals as petrogenetic indicators. Further work, however, remains on the thermodynamic characterization of solid solutions in this complex system. Hopefully, binary Cl-OH and ternary F-Cl-OH apatite solid solutions can be synthesized so as to allow completion of work relative to the primary monovalent anion substitutions. Our laboratory is anxious to contribute to this endeavor when such samples become available.

ACKNOWLEDGMENTS

G.L.H. thanks the National Science Foundation for grant EAR-1028953, which funded purchase of the PANalytical Empyrean X-ray powder diffraction system at Lafayette College. Sincere thanks to NSF also for grant EAR-1019809 and the EXCEL Program of Lafayette College, which together funded undergraduate student research. John Wilson of the Department of Geology and Environmental Geosciences at Lafayette College provided valuable assistance in setup of our new X-ray system. We greatly appreciate provision of X-ray facilities by the Earth Sciences Department of Cambridge University, as well as generous other help that facilitated our visits over the years. Thanks to Specialty Minerals Inc., Easton, Pennsylvania, where a portion of the X-ray measurements were made. Thank you to Jeff Post, Mike Wise, and Paul Powhat of the National Museum of Natural History for providing apatite samples NMNH 144954-3 and R9498. Thank you to George Harlow of the American Museum of Natural History for providing AMNH 23101 chlorapatite. We thank Matthias Gottschalk and Georg Schettler of the GFZ-Potsdam for sharing chemical and structural data on the synthetic F-Cl apatite samples. G.L.H. appreciates valuable discussions regarding apatite structure with John Hughes (University of Vermont), and also his work as AE for this manuscript. Our sincere thanks go to Hanna Nekvasil (Stony Brook University) and Francis McCubbin (University of New Mexico) for constructive criticisms during the review of this paper.

REFERENCES CITED

Boyce, J.W., Liu, Y., Rossman, G.R., Guan, Y., Eiler, J.M., Stolper, E.M., Taylor, L.A. (2010) Lunar apatite with terrestrial volatile abundances. Nature, 466, 466–469.

Cherniak, D.J. (2000) Rare earth element diffusion in apatite. Geochimica et Cosmochimica Acta, 64, 3871–3885.

Ewing, R.C., and Wang, L.M. (2002) Phosphates as nuclear waste forms. In M.J. Kohn, J. Rakovan, and J.M. Hughes, Eds., Phosphates: Geochemical, Geobiological, and Materials Importance, 48, p. 673–699. Reviews in Mineralogy and Geochemistry, Mineralogical Society of America, Chantilly, Virginia.

Gross, K.A., and Berndt, C.C. (2002) Compositions of the apatitegroup minerals: Substitution mechanisms and controlling factors. In M.J. Kohn, J. Rakovan, and J.M. Hughes, Eds., Phosphates: Geochemical, Geobiological, and Materials Importance, 48, p. 631–672. Reviews in Mineralogy and Geochemistry, Mineralogical Society of America, Chantilly, Virginia.

Gross, J., Filiberto, J., and Bell, A.S. (2013) Water in the martian interior: Evidence for terrestrial MORB mantle-like volatile contents from hydroxyl-rich apatite in olivine-phyric shergottite NWA 6234. Earth and Planetary Science Letters, 369, 120–128.

Holland, T.J.B., and Redfern, S.A.T. (1997) Unit-cell refinement: Changing the dependent variable, and use of regression diagnostics. Mineralogical Magazine, 61, 65–77.

Hounslow, A.W., and Chao, G.Y. (1970) Monoclinic chlorapatite from Ontario. Canadian Mineralogist, 10, 252–259.

Hovis, G.L., and Harlov, D. (2010) Solution calorimetric investigation of fluorchlorapatite crystalline solutions. American Mineralogist, 95, 946–952.

Hovis, G.L., McCubbin, F.M., Nekvasil, H., Ustunisik, G., Woerner, W.R., and Lindsley, D.H. (2014a) A novel technique for fluorapatite synthesis and the thermodynamic mixing behavior of F-OH apatite crystalline solutions. American Mineralogist, 99, 890–897.

Hovis, G.L., Scott, B.T., Altomare, C.M., Leaman, A.R., Morris, M.D., and Tomaino, G.T. (2014b) Thermal expansion of fluorapatite-hydroxylapatite crystalline solutions. American Mineralogist, 99, 2171–2175.

Hughes, J.M., and Rakovan, J. (2002) The crystal structure of apatite. In M.J. Kohn, J. Rakovan, and J.M. Hughes, Eds., Phosphates: Geochemical, Geobiological, and Materials Importance, 48, p. 1−12. Reviews in Mineralogy and Geochemistry, Mineralogical Society of America, Chantilly, Virginia.

Hughes, J.M., Cameron, M., and Crowley, K.D. (1989) Structural variations in natural F, OH, and Cl apatites. American Mineralogist, 74, 870–876.

Hughes, J., Nekvasil, H., Ustunisik, G., Lindsley, D.H., Coraor, A.E., Vaughn, J., Phillips, B.L., McCubbin, F.M., and Woerner, W. (2014) Solid solution in the fluorapatite-chlorapatite binary system: High-precision crystal structure refinements of synthetic F-Cl apatite. American Mineralogist, 99, 369–376.

Jones, R.H., McCubbin, F.M., Dreeland, L., Guan, Y., Burger, P.V., and Shearer, C.K. (2014) Phosphate minerals in LL chondrites: A record of the action of fluids during metamorphism on ordinary chondrite parent bodies. Geochimica et Cosmochimica Acta, 132, 120–140.

Knudsen, A.C., and Gunter, M.E. (2002) Sedimentary phosphorites—An example: Phosphoria formation, southeastern Idaho, USA. In M.J. Kohn, J. Rakovan, and J.M. Hughes, Eds., Phosphates: Geochemical, Geobiological, and Materials Importance, 48, p. 363−390. Reviews in Mineralogy and Geochemistry, Mineralogical Society of America, Chantilly, Virginia.

Mackie, P.E., Elliott, J.C., and Young, R.A. (1972) Monoclinic structure of synthetic $Ca_5(PO)_4Cl$, chlorapatite. Acta Crystallographica B, 28, 1840–1848.

McCubbin, F.M., Steele, A., Hauri, E.H., Nekvasil, H., Yamashita, S., and Hemley, R.J. (2010a) Nominally hydrous magmatism on the Moon. Proceedings of the National Academy of Science, 107, 11223–11228.

McCubbin, F.M., Steele, A., Nekvasil, H., Schnieders, A., Rose, T., Fries, M., Carpenter, P.K., and Jolliff, B.L. (2010b) Detection of structurally bound hydroxyl in fluorapatite from Apollo mare basalt 15058,128 using TOF-SIMS. American Mineralogist, 95, 1141–1150.

McCubbin, F.M., Jolliff, B.L., Nekvasil, H., Carpenter, P.K., Zeigler, R.A., Steele, A., Elardo, S.M., and Lindsley, D.H. (2011) Fluorine and chlorine abundances in lunar apatite: Implications for heterogeneous distributions of magmatic volatiles in the lunar interior. Geochimica et Cosmochimica Acta, 75, 5073–5093.

McCubbin, F.M., Hauri, E.H., Elardo, S.M., Vander Kaaden, K.E., Wang, J., and Shearer, C.K. (2012) Hydrous melting of the martian mantle produced both depleted and enriched shergottites. Geology, 40, 683–686.

Pan, Y., and Fleet, M.E. (2002) Compositions of the apatitegroup minerals: Substitution mechanisms and controlling factors. In M.J. Kohn, J. Rakovan, and J.M. Hughes, Eds., Phosphates: Geochemical, Geobiological, and Materials Importance, 48, p. 13−50. Reviews in Mineralogy and Geochemistry, Mineralogical Society of America, Chantilly, Virginia.

Parrish, W. (1953) X-ray reflection angle tables for several standards. Technical Report No. 68, Philips Laboratories Incorporated, Irvington on Hudson, New York.

Patiño Douce, A.E., and Roden, M.F. (2006) Apatite as a probe of halogen and water fugacities in the terrestrial planets. Geochimica et Cosmochimica Acta, 70, 3173–3196.

Piccoli, P.M., and Candela, P.A. (2002) Apatite in igneous systems. In M.J. Kohn, J. Rakovan, and J.M. Hughes, Eds., Phosphates: Geochemical, Geobiological, and Materials Importance, 48, p. 255−292. Reviews in Mineralogy and Geochemistry, Mineralogical Society of America, Chantilly, Virginia.

Prener, J.S. (1967) The growth and crystallographic properties of calcium fluor- and chlorapatite crystals. Solid State Science, 114, 77–83.

Schettler, G., Gottschalk, M., and Harlov, D.E. (2011) A semi-micro wet chemical method for apatite analysis and its application to the crystal chemistry of fluorapatite-chlorapatite solid solutions. American Mineralogist, 96, 138–152.

Spear, F.S., and Pyle, J.M. (2002) Apatite, monazite, and xenotime in metamorphic rocks. In M.J. Kohn, J. Rakovan, and J.M. Hughes, Eds., Phosphates: Geochemical, Geobiological, and Materials Importance, 48, p. 293−336. Reviews in Mineralogy and Geochemistry, Mineralogical Society of America, Chantilly, Virginia.

Young, E.J., and Munson, E.L. (1966) Fluor-chlor-oxy-apatite and sphene from crystal lode pegmatite near Eagle, Colorado. American Mineralogist, 51, 1476–1493.

Young, E.J., Myers, A.T., Munson, E.L., and Conklin, N.M. (1969) Mineralogy and geochemistry of fluorapatite from Cerro de Mercado, Durango, Mexico. U.S. Geological Survey Professional Paper 650-D, D84–D93.

MANUSCRIPT RECEIVED AUGUST 26, 2014
MANUSCRIPT ACCEPTED NOVEMBER 8, 2014
MANUSCRIPT HANDLED BY JOHN HUGHES